J. CHEM. SOC. FARADAY TRANS., 1994, 90(21), 3323–3330

Time-resolved Microwave Conductivity

Part 2.—Quantum-sized TiO_2 and the Effect of Adsorbates and Light Intensity on Charge-carrier Dynamics

Scot T. Martin, Hartmut Herrmann† and Michael R. Hoffmann*
W. M. Keck Laboratories, California Institute of Technology, Pasadena, CA 91125, USA

Charge-carrier recombination dynamics after a pulsed laser excitation are investigated by time-resolved microwave conductivity (TRMC) for quantum-sized (Q-) TiO_2 and P25, a bulk-phase TiO_2. Adsorbed scavengers such as HNO_3, HCl, $HClO_4$, isopropyl alcohol, *trans*-decalin, tetranitromethane, and methyl viologen dichloride result in different charge-carrier recombination dynamics for Q-TiO_2 and P25. The differences include a current doubling with isopropyl alcohol for which electron injection into Q-TiO_2 is much slower than into P25 and relaxation of the selection rules of an indirect-bandgap semiconductor due to size quantization. However, the faster interfacial charge transfer predicted for Q-TiO_2 due to a 0.2 eV gain in redox overpotentials is not observed. The effect of light intensity is also investigated. Above a critical injection level, fast recombination channels are opened, which may be a major factor resulting in the dependence of the steady-state photolysis quantum yields on $I^{-1/2}$. The fast recombination channels are opened at lower injection levels for P25 than for Q-TiO_2, and a model incorporating the heterogeneity of surface-hole traps is presented.

When the radius of a colloidal semiconductor particle falls below the exciton radius (1–10 nm), size-quantization effects appear.[1–6] Colloidal TiO_2 can be prepared in the size-quantized regime by sol–gel synthesis methods.[7–9] Over the last several years, we have been investigating the feasibility of using size-quantized TiO_2 as a strategy to improve the quantum efficiencies of redox transformations.[10–14] In particular, ultra-bandgap illumination ($\lambda < 388$ nm) of a suspension of TiO_2 particles results in the stoichiometric oxidation of many chlorinated hydrocarbons to CO_2 and HCl.[15–20] A generalized photoelectrochemical mechanism involving the major processes can be written as follows:[21–24]

photogeneration: $TiO_2 + h\nu \rightarrow e^- + h^+$ (1)

carrier trapping:

$$>Ti^{4+}-O^{2-}H + e^- \leftrightarrow >Ti^{3+}-O^{2-}H \quad (2)$$

$$>Ti^{4+} - O^{2-}H + h^+ \rightarrow >Ti^{4+}-O^{\cdot-}H \quad (3)$$

recombination:

$$e^- + >Ti^{4+} - O^{\cdot-}H \rightarrow >Ti^{4+}-O^{2-}H \quad (4)$$

substrate oxidation:

$$>Ti^{4+}-O^{\cdot-}H + R \rightarrow >Ti^{4+}-O^{2-}H + R^{\cdot+} \quad (5)$$

substrate hydroxylation:

$$>Ti^{4+}-O^{\cdot-}H + R \rightarrow >Ti^{4+} + {}^{+\cdot}RO^{2-}H \quad (6)$$

$$>Ti^{4+} + H^+O^{2-}H \rightarrow >Ti^{4+}-O^{2-}H + H^+ \quad (7)$$

electron deactivation:

$$>Ti^{3+}-O^{2-}H + O_2 \rightarrow >Ti^{4+}-O^{2-}H + O_2^{\cdot-} \quad (8)$$

$$O_2^{\cdot-} + H^+ \rightarrow HO_2^{\cdot} \quad (9)$$

Critical steps of the photoelectrochemical mechanism of eqn. (1)–(9) have been investigated by the transient absorption spectra obtained following laser flash photolysis of transparent colloidal TiO_2.[24–31] Most investigators have assumed that conclusions reached regarding colloidal TiO_2 are applicable to larger bulk-phase TiO_2 particles. In the present study, the basis of this assumption is investigated by using TRMC measurements, which do not discriminate by crystallite size,[10,32–39] to compare the photoelectrochemical mechanisms of quantum-sized TiO_2 and bulk-phase TiO_2 (Degussa P25).[17–20,40–63] We have recently reported that the relative steady-state quantum efficiencies obtained with these two different forms of TiO_2 depend upon the specific reaction mechanisms involving the electron donors (*e.g.* direct hole transfer or hydroxyl radical attack).[10] Flash photolysis–TRMC experiments are used to compare the charge-carrier dynamics of Q-TiO_2 and P25 TiO_2 as functions of the acid used in the sol–gel synthesis, of the charge-carrier scavengers present at the particle interfaces and of light intensity.

† Present address: Institut für Physikalische und Theoretische Chemie der Universität, GH Essen, Germany.

Experimental

Preparation and Characterization

Powders of Q-sized TiO_2 particles were synthesized by the controlled hydrolysis of titanium(IV) tetraisopropoxide in the presence of HCl, HNO_3, or $HClO_4$ according to procedures described previously.[7,10] The sol–gel suspension from $HClO_4$ was neutralized with NaOH to pH 3.0 in order to obtain a powder. A powder containing methyl viologen (MV) dichloride hydrate (Aldrich) was obtained by rotary evaporation of a resuspension of TiO_2–HNO_3 mixed with MV. Dry powders of P25 were obtained by the rotary evaporation of suspensions (1.44 g l^{-1}, pH 1.5) in HNO_3, HCl, $HClO_4$ or MV. P25 and Q-TiO_2 were supported with several drops of *trans*-decalin (T) except for the preparations containing isopropyl alcohol (ISP) and tetranitromethane (TM), which were prepared at the time of measurement by adding several drops to the powders.

The Q-TiO_2 particles were characterized as described previously.[10] high-resolution transmission electron microscopy (HRTEM) lattice spacing images and X-ray diffraction (XRD) Scherrer line broadening showed the size distribution of the particles was between 2 and 4 nm. The electron diffraction (ED) and XRD patterns of the TiO_2 particles were characteristic of anatase. A blue shift of the absorption onset to 345 nm (3.6 eV) was observed. The absorption coefficient at 308 nm was 2.9×10^4 cm^{-1}. Degussa P25 particles, which were composed of 30 nm crystallites consisting of 80% anatase and 20% rutile, aggregated to form 1 μm particles.[41,42]

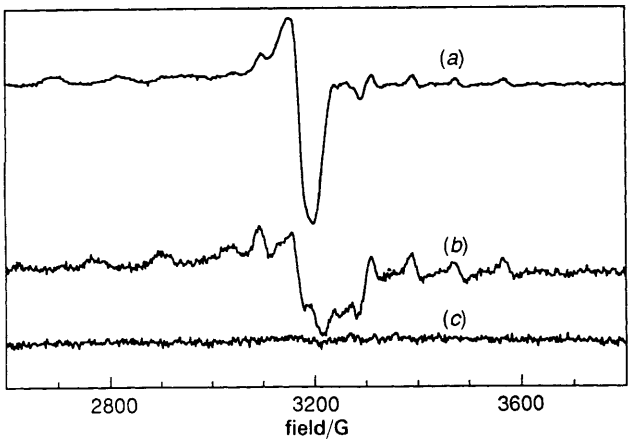

Fig. 1 EPR spectra obtained at 77 K for sol–gel preparations of size-quantized TiO_2 in (*a*) HNO_3, (*b*) HCl and (*c*) $HClO_4$

EPR Measurements

An E-line Century X-band Spectrometer (Varian, Palo Alto, CA) was used to record the first-derivative EPR spectra at 77 K. $CuSO_4$ was used as a calibration standard. The TiO_2 samples were prepared as gels (*ca.* 10 g l^{-1}) for the EPR analysis.

TRMC Measurements

The TRMC apparatus is described in the previous paper.[10] In a typical TRMC experiment separated charge-carriers, which are generated by a laser pulse, lead to a perturbation of the initial microwave absorbance. The temporal decay of the conductivity signal (*i.e.* microwave absorbance) reflects the lifetime of the photogenerated carriers and is given by the following equation

$$\frac{d\sigma}{dt} = \mu_{e_{cb}^-}\frac{d[e_{cb}^-]}{dt} + \mu_{e_T^-}\frac{d[e_T^-]}{dt} + \mu_{h_{vb}^+}\frac{d[h_{vb}^+]}{dt} + \mu_{h_T^+}\frac{d[h_T^+]}{dt} \quad \text{(I)}$$

where σ is the conductivity, e_T^- is a trapped electron, h_T^+ is a trapped hole, e_{cb}^- is a conduction-band electron, and h_{vb}^+ is a valence-band hole. The hole terms in eqn. (I) are negligible on the timescales of Fig. 1–4 (later) due to fast hole trapping at immobile surface hydroxy groups.[10] In this case, the conductivity is due to the two-electron terms in eqn. (12), and the conductivity decay corresponds to the recombination [eqn. (4)] or emission of electrons to substrate [eqn. (10)–(13)]

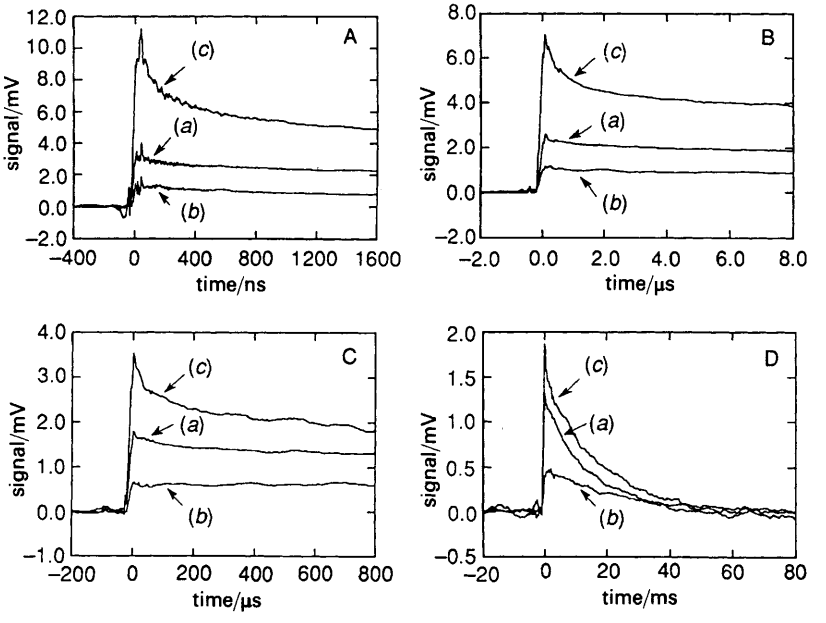

Fig. 2 Effect of (*a*) HNO_3, (*b*) HCl and (*c*) $HClO_4$ on the conductivity decays of Degussa P25 supported in T. A, 200 ns div^{-1} timebase; B, 2 μs div^{-1} timebase; C, 200 μs div^{-1} timebase; D, 10 ms div^{-1} timebase.

Table 1 Relative initial carrier concentrations and conductivity decay half-lives

	relative initial carrier concentration		half-life					
adsorbate	P25	Q-TiO_2	P25			Q-TiO_2		
$HClO_4$	11.2	2.1	750 ns	25 μs	1.6 ms	1.6 μs	800 μs	11 ms
HNO_3	3.6	3.0	8.0 μs	4.3 ms		2.8 ms	6.3 ms	
HCl	1.4	1.7	35 μs	8.7 ms		2.8 μs	110 μs	8.3 ms
T	4.3	3.0	7.9 μs	5.9 ms		2.8 ms		
ISP	6.8	1.1	3.5 μs	650 μs	8.7 ms	19 ms		
TM	4.3	n/a	230 ns	2.2 μs	51 μs	n/a		
MV	5.0	0.9	95 ns	1.1 μs		13 ms		

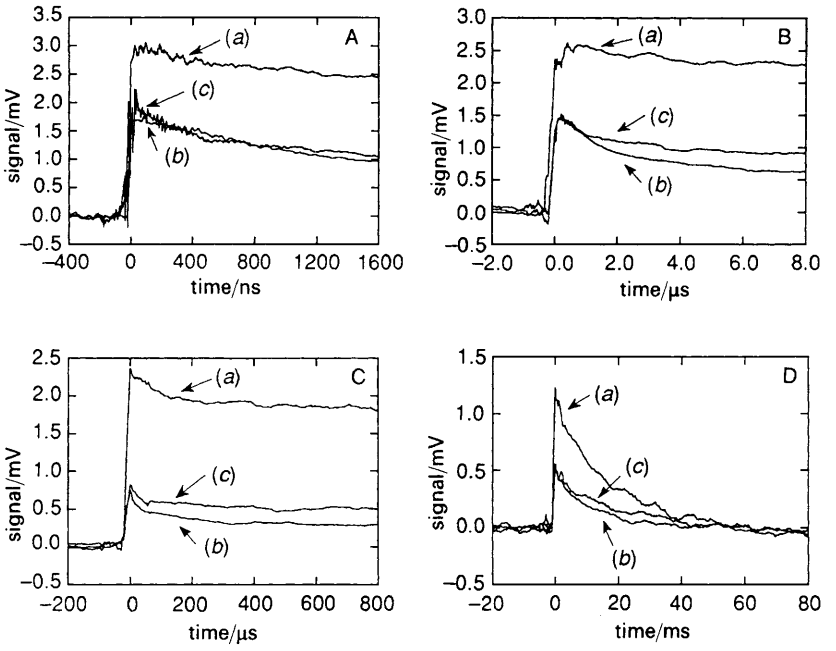

Fig. 3 Effect of (*a*) HNO_3, (*b*) HCl and (*c*) $HClO_4$ on the conductivity decays of Q-TiO_2 supported in T. A, 200 ns div^{-1} timebase. B, 2 μs div^{-1} timebase. C, 200 μs div^{-1} timebase; D, 10 ms div^{-1} timebase.

interfacial electron transfer from the conduction-band:

substrate reduction: $e^- + Ox \rightarrow O^{\bullet -}$ (10)

short circuit: $e^- + Red^{\bullet +} \rightarrow Red$ (11)

interfacial electron transfer mediated by a surface trap:

substrate reduction:

$$>Ti^{3+}-O^{2-}H + Ox \rightarrow >Ti^{4+}-O^{2-}H + Ox^{\bullet -} \quad (12)$$

short-circuit:

$$>Ti^{3+}-O^{2-}H + Red^{\bullet +} \rightarrow >Ti^{4+}-O^{2-}H + Red \quad (13)$$

The recombination channel [eqn. (4)] is exhausted for $t \gg 10$ ns because all the holes have escaped the particle [eqn. (5) and (6)].[10] The conductivity decay is then due solely to interfacial electron transfer to the adsorbed substrate [eqn. (10)–(13)], and the microwave conductivity at 100 ns is due to the fraction of charge pairs that have not recombined [eqn. (4)] or transferred immobile sites [eqn. (3) and (5)–(13)].[10]

Results

The EPR spectra of Q-TiO_2 prepared in HNO_3, $HClO_4$, or HCl are shown in Fig. 1. The effects of adsorbed HNO_3, $HClO_4$, and HCl on the conductivity decays of P25 and Q-

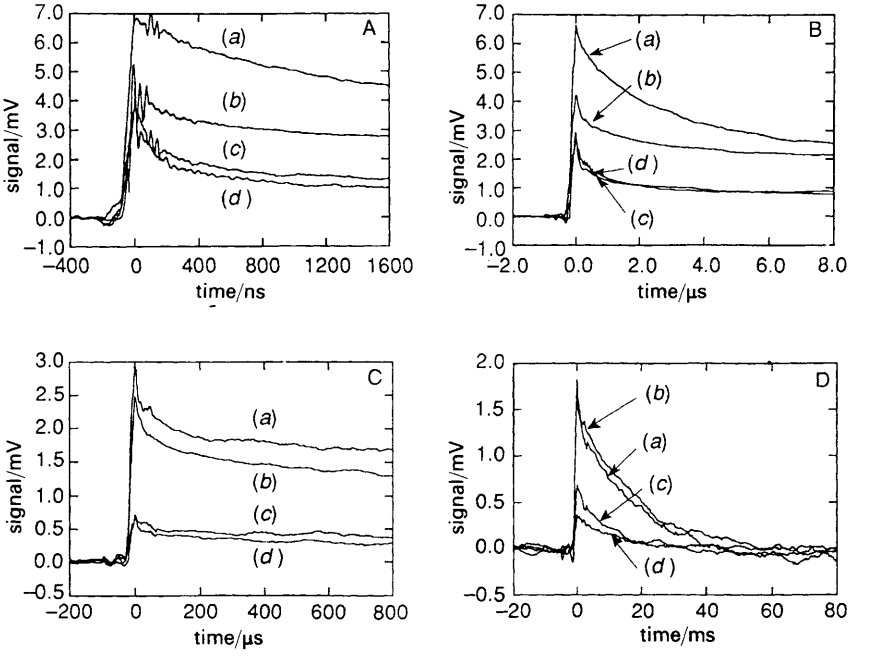

Fig. 4 Effect of (*a*) ISP, (*b*) T, (*c*) TM and (*d*) MV on the conductivity decays of Degussa P25. A, 200 ns div^{-1} timebase; B, 2 μs div^{-1} timebase; C, 200 μs div^{-1} timebase; D, 10 ms div^{-1} timebase.

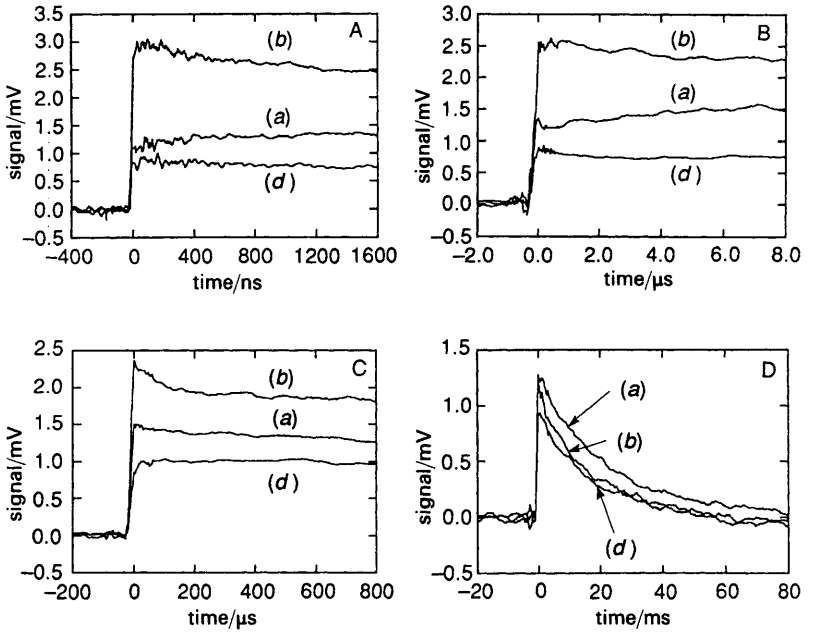

Fig. 5 Effect of (*a*) ISP, (*b*) T and (*d*) MV (supported in T) on the conductivity decays of Q-TiO_2 prepared in HNO_3. A, 200 ns div^{-1} timebase; B, 2 μs div^{-1} timebase; C, 200 μs div^{-1} timebase; D, 10 ms div^{-1} timebase.

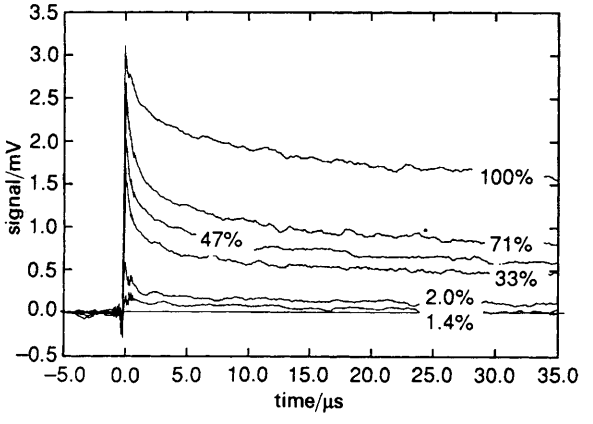

Fig. 6 Effect of the incident laser pulse energy (100% = 4.9 mJ $pulse^{-1}$) on the conductivity decays of Degussa P25 supported in *trans*-decalin on the 2 μs div^{-1} timebase

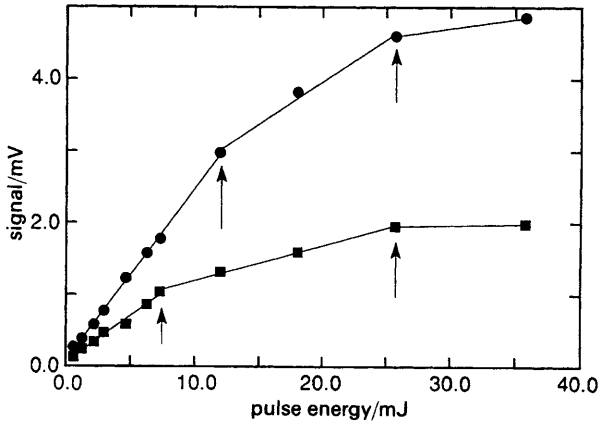

Fig. 8 Effect of the incident laser pulse energy on the initial (●, 100 ns) and the residual (■, 15 μs) conductivity of Q-TiO_2 prepared in $NaClO_4$ and T

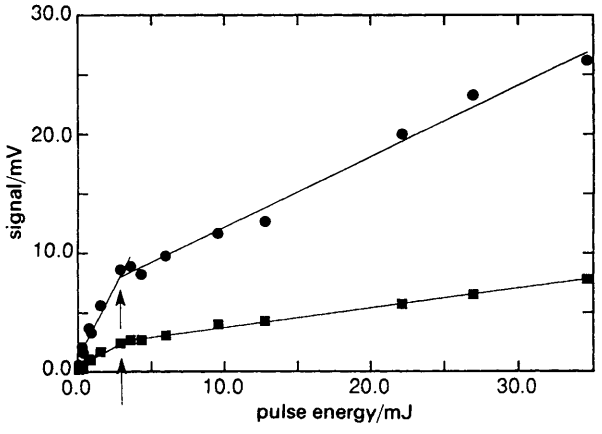

Fig. 7 Effect of the incident laser pulse energy on the initial (●, 100 ns) and the residual (■, 15 μs) conductivity of Degussa P25 prepared in $NaClO_4$ and T

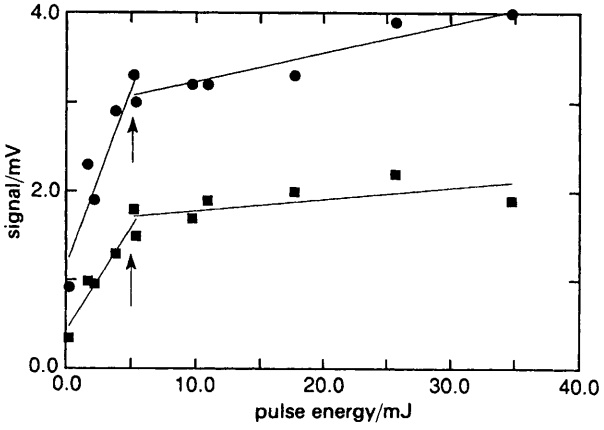

Fig. 9 Effect of the incident laser pulse energy on the initial (●, 100 ns) and the residual (■, 15 μs) conductivity of Degussa P25 prepared in HNO_3 and T

TiO_2 are shown in Fig. 2 and 3 while the corresponding conductivity decays of P25 and Q-TiO_2 in the presence of T, ISP, TM and MV^{2+} are shown in Fig. 4 and 5. The relative initial charge-carrier concentrations (Table 1), which are determined at 100 ns, are proportional to the conductivity signal strengths observed in Fig. 2(a)–5(a).

The time-resolved conductivity signals of P25 supported in T were found to be a function of the incident pulse energy, as shown in Fig. 6. Similar results were obtained for different adsorbate systems (*i.e.* ClO_4^-, and Cl^- in T), as shown in Fig. (7)–(9) in which the initial charge-carrier concentrations at 100 ns and 15 μs are plotted as functions of the laser pulse energy (*i.e.* the charge-carrier injection level). For P25 prepared in $NaClO_4$ and T (Fig. 7) the carrier concentrations at 100 ns and 15 μs appear to have a lower rate of increase above 4 mJ for a similar increase in injection level. In the presence of $NaClO_4$ and T (Fig. 8), the critical injection level for Q-TiO_2 shifts to *ca.* 10 mJ, and a second critical level at 25 mJ is also apparent. Samples of P25 prepared in HNO_3 and T (Fig. 9) appear to have critical injection levels at 5 mJ and lower saturation levels than similar samples prepared in $NaClO_4$ (Fig. 7).

Discussion

Charge-carrier recombination

The fate of the majority of photoexcited charge-carrier pairs in undoped ultra-small particulate semiconductor particles is rapid recombination[20] since the instantaneous charge-carrier concentrations from the laser pulse are of the order of 10^{21} cm^{-3}. At these concentrations, the higher energy states of the energy bands are populated and symmetry-allowed (*i.e.* direct) bandgap recombination in TiO_2 is facilitated. Fast recombination also occurs between free holes and trapped electrons [eqn. (4)].[10,24] Both these channels are exhausted within the time-resolution of our experiment. When the residual carrier-level concentration falls to 10^{18} cm^{-3}, the Fermi level is moved out of degeneracy and the residual conductivity is detected by our measurement system. A carrier concentration of *ca.* 10^{18} cm^{-3} should be representative of the steady-state concentrations of accumulated charge carriers in CW photolysis experiments.[64]

Fast charge-pair recombination rates are further enhanced in size-quantized semiconductor particles owing to the mixing of states that relaxes the selection rules for an indirect transition.[65–69] This latter effect of size quantization is clearly illustrated in the data summarized in Table 1. For all sorbates (electron acceptors and electron donors) the concentration of charge-carriers is lower in Q-TiO_2 than in P25 after 100 ns. These experiments suggest that indirect-bandgap semiconductors in the Q-sized domain are less photoefficient redox catalysts owing to inherently faster rates of charge-carrier recombination. This photophysical effect offsets the predicted gains associated with higher thermodynamic driving forces for interfacial electron transfer.

Surface Structures

The EPR spectra shown in Fig. 1 suggest the formation of radical species on the surface of the TiO_2 particles. The species may include $>Ti^{III}-Cl$, $>Ti^{III}-ONO_2$, $>Ti^{IV}-Cl^{\bullet}$ and $>Ti^{IV}-ONO_2^{\bullet}$. However, the radicals present in the sample constitute only 1% of the atoms, as indicated by a comparison of the integrated intensity of the EPR signals to the $CuSO_4$ standard. The observed radicals suggest that the acid anions interact with the surface of the particle and that the bulk of the anions speciate as $>Ti^{IV}-Cl$, $>Ti^{IV}-ONO_2$ and $>Ti^{IV}-OClO_3$.

Fluctuating energy Level Model

The observed differences as a function of added acids (Fig. 2 and 3) suggest that photogenerated charge carriers undergo interfacial charge transfer to the acid anions on the surface of the TiO_2 particles. The kinetics of the interfacial charge transfer can be understood in terms of the fluctuating-energy model proposed by Gerischer.[70] The one-electron oxidation potentials of the acid adsorbates under standard conditions are as follows:[71]

$$Cl^- \leftrightarrow Cl^{\bullet} + e^-; \qquad E^\circ = -2.6\ V \qquad (14)$$

$$NO_3^- \leftrightarrow NO_3^{\bullet} + e^-; \qquad E^\circ = -2.3\ V \qquad (15)$$

$$OH^- \leftrightarrow {}^{\bullet}OH + e^-; \qquad E^\circ = -1.9\ V \qquad (16)$$

Although the one-electron oxidation potential for perchlorate is not known, we assume that the value lies between 2.0 and 3.0 eV based upon comparison with eqn. (14) and (15). The oxidation potential of the surface-bound hydroxide anion [*i.e.* eqn. (3)] can be estimated also from eqn. (17); it has been reported to be −1.5 V.[21] Thus, the oxidation of the adsorbed acids can take place only from direct valence-band hole transfer since the E°_{rxn} ($^{\bullet}OH$–acid anion) value <0 (*i.e.* $\Delta G^\circ \gg 0$).

The corresponding two-electron reduction potentials for nitrate and perchlorate are as follows:[72]

$$NO_3^- + 2e^- + 3H^+ \leftrightarrow HNO_2 + H_2O; \qquad E^\circ = +0.9\ V \qquad (17)$$

$$ClO_4^- + 2e^- + 2H^+ \leftrightarrow ClO_3^- + H_2O; \qquad E^\circ = +1.2\ V \qquad (18)$$

Within ±0.2 V, a conduction-band electron has a reduction potential of −0.3 V [eqn. (10) and (11)] and a valence-band hole has a reduction potential of 2.9 V [eqn. (3)] at pH 0. In these calculations, we used the constraints that the conduction-band edge for TiO_2 is 0.1–0.2 V negative of the flatband potential and that the bandgap of anatase is 3.2 eV. The flatband potential has been determined to be −0.1[27] and −0.2 V[73] *vs.* NHE at pH 0 for colloidal TiO_2. The size-quantization effects in Q-TiO_2 increase the bandgap by 0.4 eV.[9] This increase corresponds to a shift in the reduction potential of the conduction-band electron to −0.5 V and of the valence-band hole to +3.1 eV for Q-TiO_2 at pH 0. Since Degussa P25 is predominantly anatase,[41] its band edges are at −0.3 and 2.9 V at pH 0.

The apparent reduction potentials of trapped charge carriers are difficult to estimate. In the case of a trapped electron, Ti^{III} is 0.2–0.5 eV negative of the conduction-band edge at zero surface charge, E°_{cb}, of rutile.[74–76] Using $E^\circ_{cb} = -0.3$ V *vs.* NHE and $pH_{zpc} = 5.8$,[77] the reduction potential of a trapped electron [eqn. (8), (12) and (13)] is *ca.* −0.25 V *vs.* NHE. Because the trapped electron is localized, the reduction potential is the same for both Q- and P25 TiO_2. The trap is 50 mV below E_{cb} of P25, in agreement with other suggestions,[35] and is 250 mV below E_{cb} of Q-TiO_2. The reduction potential of a trapped hole [eqn. (6) and (7)] is +1.5 V, as discussed for eqn. (16).

The acid anions (Cl^-, NO_3^- and ClO_4^-) are chemisorbed onto the surface of TiO_2 by ligand substitution of surface hydroxy groups and by electrostatic attraction at pH < 6.8. The one-electron oxidation potentials [eqn. (14)–(16)] indicate that the acid anions at the TiO_2 surface are thermodynamically less capable of hole capture than surface hydroxide but may still serve as good hole traps [eqn. (3)] owing to the high overlap between the energy levels of the acid anions and the valence-band hole for $0.5 < \lambda/eV < 1.0$ where λ is the reorganization energy.[77,78] Although OH^- and Cl^- cannot be further reduced, NO_3^- and ClO_4^- undergo multi-electron

reductions [eqn. (17) and (18)] and thus may serve as effective electron traps.

Inorganic Donors and Acceptors

Interfacial charge transfers to the acid anion adsorbates occur on the ps and short ns timescales and compete with interfacial recombination processes. This effect is clearly seen in Table 1, in which the initial charge-carrier concentrations appear to be unique for each adsorbate. In the case of HCl, the chemisorbed Cl^- anion directly scavenges valence-band holes [eqn. (19)] within 10 ns in direct competition with surface OH^- [eqn. (3)]:[26]

$$>Ti^{4+}-Cl^- + h^+ \rightarrow >Ti^{4+}-Cl^{\bullet} \quad (19)$$

After formation, the surface chloride radical may open a second channel for charge-carrier recombination as follows:

$$e^- + >Ti^{4+}-Cl^{\bullet} \rightarrow >Ti^{4+}-Cl^- \quad (20)$$

The relatively low carrier concentrations observed at 100 ns indicate that the cross-section for electron capture by a surface chloride radical [eqn. (20)] is greater than that for a surface hydroxy group [eqn. (4)]. This observation could be explained, in part, by the relative differences in electronegativity for OH^- and Cl^-.

Since nitrate and perchlorate serve as both potential electron scavengers and hole scavengers, three scenarios are possible to explain their effects: (*a*) $>Ti^{IV}-ONO_2$ and $>Ti^{IV}-OClO_3$ could act as fast hole scavengers; (*b*) they could act primarily as fast electron scavengers or (*c*) they could act equally with respect to the trapping of both charge types. In case (*a*) fast hole trapping exhausts the reservoir of electron-accepting species and the conductivity signal is proportional to the concentration of electrons. Case (*b*) is the opposite of case (*a*), *i.e.* the conductivity signal is due to free holes. In case (*c*) electrons and holes are equally separated on the surface of the semiconductor particle while the charge carriers remaining within the particle recombine rapidly and thus no residual conductivity is observed at 100 ns. As shown in Fig. 2, case (*c*) does not appear to occur. Thus, preferential trapping of one carrier type as in (*a*) or (*b*) appears to take place. Although processes (*a*) and (*b*) are not directly distinguishable in our experiment, we will attempt to show that interfacial electron transfer does not occur significantly within the time-resolution of the experiment (*vide infra*). In this case, the conductivity signal should be due to electrons as in (*a*).

The relatively high electron-charge-carrier concentrations shown in Fig. 3(*a*) for P25 in the presence of $HClO_4$ suggest that the cross-sections for hole capture by $>Ti^{IV}-OClO_3$ or $>Ti^{IV}-OH$ are comparable while $>Ti^{IV}-OClO_3^{\bullet}$ has a lower cross-section for electron capture than $>Ti^{IV}-OH^{\bullet}$. In the case of Q-TiO_2, the electron concentration in the presence of $HClO_4$ shows that the cross-section for electron capture by $>Ti^{IV}-ClO_4^{\bullet}$ increases relative to P25. The lower charge-carrier concentrations observed in the presence of HCl for P25 as compared with Q-TiO_2 indicate that valence-band hole-capture rates of $>Ti^{IV}-Cl$ [eqn. (19)] are greater for P25 than for Q-TiO_2. In this case, more carriers are short-circuited by conduction-band electron transfer to $>Ti^{IV}-Cl^{\bullet}$ [eqn. (20)] for P25 than for Q-TiO_2, and thus the residual charge-carrier concentration at 100 ns is greater for Q-TiO_2 than for P25 (Table 1).

Organic Donors and Acceptors

TM and MV^{2+} are known to serve readily as electron scavengers in TiO_2 systems[7,27,31] while T, a saturated bicyclic hydrocarbon, and ISP serve as surface hole scavengers.[7,10,79] The measured charge-carrier concentrations at 100 ns in P25 are comparable in the presence of MV^{2+}, TNM, ISP and T. If fast interfacial electron transfer were taking place to TM and MV^{2+}, then the carrier concentrations at 100 ns would be expected to be reduced. The first half-lives for the charge carriers in the presence of MV^{2+}, TNM, ISP and T are 95 ns, 230 ns, 3.5 μs and 7.9 μs, respectively. Thus, we conclude that, even in the presence of fast electron acceptors, interfacial electron transfer takes place primarily at timescales $\geqslant$ 100 ns.

In the presence of electron acceptors (TNM and MV^{2+}), the conductivity decays flatten on the ms timescale, as shown in Fig. 4(*b*) and (*c*) and Fig. 5(*b*) and (*c*); this effect suggests that electron transfer does not take place on this timescale. Electron transfer to TNM and MV^{2+} takes place during the first 500 ns, as shown in Fig 4(*a*) and 5(*a*). After that time, the surface substrate is exhausted and further electrons do not escape the particle until fresh substrate diffuses to the surface, as shown in Fig. 4(*d*) and 5(*d*).[10]

The increasing charge-carrier concentrations seen in Fig. 5(*a*) and (*b*) suggest that back electron injection from ISP into Q-TiO_2 takes place. The current-doubling effect occurs when a one-electron oxidant such as ISP produces a radical that can inject an electron into the conduction band of TiO_2 as follows:[7]

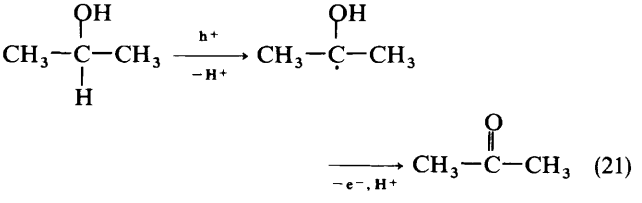

(21)

This effect is absent in Fig. 4(*a*) and (*b*) for P25. However, the highest initial conductivity signal for P25 is observed when ISP is the electron donor, which supports the argument that back electron injection takes place much more quickly than in Q-TiO_2. A slower rate for Q-TiO_2 may be due to the 0.2 eV shift to the negative of the conduction-band edge of Q-TiO_2, which should slow electron injection. Slower electron injection rates into Q-TiO_2 may also arise from a drop in the electron-transfer probability due to a higher surface density of hydroxy groups that sterically hinder surface Ti^{IV}, which is the likely site for electron injection into the conduction band. The sol–gel preparation method is expected to result in higher surface densities of hydroxy groups for Q-TiO_2 than for P25, which is prepared by flame hydrolysis.

Light Intensity Effects

The observed decay rates from 100 ns to 35 μs (Fig. 6) follow apparent first-order kinetics; this observation implies that the charge carriers act independently of one another at $t \leqslant 35$ μs. However, the charge-carrier concentrations at 100 ns are not directly proportional to the initial charge-carrier injection levels because fast recombination is a second-order process. The observed carrier concentrations at 100 ns give us a measure of the extent of charge-carrier recombination at $t \leqslant 100$ ns.

The charge-carrier injection level can be determined from the number of photons injected into the penetration depth of Q-TiO_2 at 308 nm:

$$I\ (cm^{-3}) = 2.3 \times 10^{17} \frac{I\ (mJ)\ \alpha\ (cm^{-1})}{h\nu\ (eV)\ A\ (mm^2)} \quad (23)$$

where I (cm^{-3}) is the injection level, I (mJ) is the pulse energy, α is the absorption coefficient, A is the cross-sectional

area, and $h\nu$ is the photon energy. In our flash photolysis system, a 4.5 mJ pulse results in *ca.* 10^{21} carriers cm^{-3}.

The slopes of the lines in Fig. 7–9 can be defined as *response factors*. The response factor is the relative change in the carrier concentration at a time, t, produced by a change in the injection level. In the absence of higher order (*i.e.* fast) recombination processes, the response factor should be high while the response factor is zero at *saturation*. The injection level at which the response factor changes is defined as the *cross-over threshold*. These thresholds (Table 2) are the injection levels at which new higher order deactivation channels are opened and they appear as discontinuities in the lines in Fig. 7–9.

The response factors in Table 2 decrease as the injection level increases, which indicates that higher injection levels result in larger quantum yields for fast recombination. In a typical CW experiment, higher light intensities are expected to raise the quantum yields for fast recombination and thus to reduce the net quantum yields for substrate oxidation and reduction. This conclusion provides evidence for our hypothesis that the quantum efficiencies for oxidation and reduction in CW photolysis fall as the square-root of absorbed light intensity ($\Phi \propto I^{-1/2}$) owing to rapid recombination at higher light intensities.[53]

The apparent discontinuities at the cross-over thresholds in Fig. 7–9 may be explained in terms of a mechanism involving two chemically distinct hole-trapping sites, S_1 and S_2, in TiO_2 that have hole-trapping cross-sections σ_1 and σ_2.[21] S_1 is most likely $OH_s^{\bullet}$ formed on a surface Ti^{IV} site and S_2 is $OH_s^{\bullet}$ formed on a surface μ-O site. We propose that $\sigma_1 \gg \sigma_2$ due to a potentially unfavourable charge balance on μ-O. The concentrations of S_1 and S_2 following an injection level of $[S_0]$ are subject to the following constraints:

$$[S_1](0) = \begin{cases} [S_0], & [S_0] < S_1 \\ S_1, & [S_0] \geqslant S_1 \end{cases}$$

$$[S_2](0) = \begin{cases} 0, & [S_0] \leqslant S_1 \\ [S_0] - S_1, & [S_0] > S_1 \end{cases} \qquad \text{(II)}$$

where $[S_1]$ and $[S_2]$ are the concentration of occupied hole traps. At the time of injection, $[S_1](0) + [S_2](0) = [S_0]$. Due to stoichiometric annihilation, $[C](t) = [S_1](t) + [S_2](t)$ for $t \ll \tau_{tht}$ where τ_{tht} is the time for interfacial hole transfer and $[C](t)$ is the concentration of electrons.

The time-dependent decay of $[S_1]$ and $[S_2]$ may be modelled as follows:

$$[C](t) = [S_1](0)\exp(-k_1 t) + [S_2](0)\exp(-k_2 t) \qquad \text{(III)}$$

$$[C](100\ \text{ns}) = m_1[S_1](0) + m_2[S_2](0) \qquad \text{(IV)}$$

where $k_{1,2}$ are the cross-sections for charge-carrier recombination [eqn. (4)] and the response factors, $m_{1,2}$, are $\exp[-k_{1,2}(100\ \text{ns})]$. A plot of the conductivity signal $[C](100\ \text{ns})$ *vs.* the injection level, $[S_0]$, under the conditions set out in eqn. (II) results in two straight lines with a discontinuity at the cross-over threshold where $[S_0] = S_1$.

The higher surface area and surface hydroxylation of Q-TiO_2 results in cross-over thresholds at an injection level five to ten times higher than P25, as shown in Table 1. The effect of HNO_3 and $HClO_4$ on the surface states of Degussa P25 is shown by the difference in cross-over thresholds and response factors. Saturation of the response factor for HNO_3 indicates that k_2 is fast. Q-TiO_2 has a second cross-over threshold, which indicates a third possible site for trapped holes.

Conclusions

We have shown that the charge-carrier dynamics of Q-TiO_2 and P25 respond differently with respect to added electron donors and acceptors and to absorbed light intensity. These effects suggest significant differences in the photoelectrochemical mechanisms for Q-TiO_2 and P25. Anions such as Cl^- affect the charge-carrier recombination processes by introducing surface states through specific adsorption as follows:

$$>Ti{-}OH + Cl^- + H^+ \rightarrow >Ti{-}Cl + H_2O \qquad (27)$$

Hence, the photoreactivity of Q-TiO_2 could be enhanced by deactivation of fast surface recombination processes.

Wide bandgap quantum-sized semiconductors such as ZnO and TiO_2 should be moving further into the Marcus inverted region[80,81] with respect to the net driving force for oxidation. However, when quantum efficiencies are limited by the rate of reduction, size quantization has been shown to yield high quantum yields for H_2O_2 production on ZnO[11] or alkene reduction on TiO_2.[82] In the case of pollutant oxidation on TiO_2, quantum efficiencies may be limited primarily by the effective rate of interfacial reduction.[83,84] However, the mixing of states in the size-quantization regime appears to enhance direct electron–hole pair recombination in indirect-bandgap semiconductors (*i.e.* TiO_2). In the size-quantization regime of TiO_2, faster electron–hole pair recombination may offset the increased driving force for interfacial reduction.

We are indebted to Prof. Nathan S. Lewis for the loan of microwave components and to Prof. Geoffrey A. Blake for the use of the excimer laser. We are grateful to ARPA and ONR {NAV 5 HFMN N0001492J1901} for financial support. S.M. is supported by a National Defence Science and Engineering Graduate Fellowship. H.H. wishes to thank NATO/DAAD for financing a research visit at the California Institute of Technology. Wonyong Choi, Dr. Amy Hoffman, Nicole Peill and Dr. Andreas Termin provided valuable support and stimulating discussion.

Table 2 Injection level cross-over thresholds and response factors

	injection level cross-over threshold /10^{-20} cm^{-3}		$= \left(\frac{\text{response factor } \Delta\text{carrier concentration}}{\Delta\text{injection level}}\right)$	
system	100 ns	15 μs	100 ns	15 μs
P25 in $NaClO_4$	<3.6	<3.6	2.4	0.7
and T	>3.6	>3.6	0.6	0.2
sol–gel Q-TiO_2 in	<14	<8.6	0.24	0.13
$NaClO_4$ and T	<25	<25	0.12	0.05
	>25	>25	0.03	0.003
P25 in HNO_3	<6.0	<6.0	0.40	0.23
and T	>6.0	>6.0	0.03	0.01

References

1 D. W. Bahnemann, *Isr. J. Chem.*, 1993, **33**, 115.
2 M. G. Bawendi, M. L. Steigerwald and L. E. Brus, *Annu. Rev. Phys. Chem.*, 1990, **41**, 477.
3 L. Brus, *Appl. Phys. A*, 1991, **53**, 465.
4 A. T. Henglein, *Curr. Chem.*, 1988, **143**, 113.
5 A. T. Henglein, *Chem. Rev.*, 1989, **89**, 1861.
6 M. L. Steigerwald and L. E. Brus, *Annu. Rev. Mater. Sci.*, 1989, **19**, 471.
7 D. Bahnemann, A. Henglein, J. Lilie and L. Spanhel, *J. Phys. Chem.*, 1984, **88**, 709.
8 J. Livage, M. Henry and C. Sanchez, *Prog. Solid State Chem.*, 1988, **18**, 259.
9 C. Kormann, D. W. Bahnemann and M. R. Hoffmann, *J. Phys. Chem.*, 1988, **92**, 5196.
10 S. T. Martin, H. Herrmann, W. Choi and M. R. Hoffmann, 1994, *J. Chem. Soc., Faraday Trans.*, **90**, 3315.
11 A. J. Hoffman, E. R. Carraway and M. R. Hoffmann, *Environ. Sci. Technol.*, 1994, **28**, 776.
12 A. J. Hoffman, G. Mills, H. Yee and M. R. Hoffmann, *J. Phys. Chem.*, 1992, **96**, 5546.
13 A. J. Hoffman, H. Yee, G. Mills and M. R. Hoffmann, *J. Phys. Chem.*, 1992, **96**, 5540.
14 E. R. Carraway, A. J. Hoffman and M. R. Hoffmann, *Environ. Sci. Technol.*, 1994, **28**, 786.
15 D. W. Bahnemann, D. Bockelmann and R. Goslich, in *Solar Energy Materials*, Elsevier, North-Holland, 1991, p. 564.
16 M. A. Fox and M. T. Dulay, *Chem. Rev.*, 1993, **93**, 341.
17 *Homogeneous and Heterogeneous Photocatalysis*, ed. E. Pelizzetti and N. Serpone, Reidel, Dordrecht, 1986.
18 *Photoelectrochemistry, Photocatalysis and Photoreactors*, ed. M. Schiavello, Reidel, Dordrecht, 1985.
19 *Photocatalysis and Environment: Trends and Applications*, ed. M. Schiavello, Kluwer, Dordrecht, 1988.
20 *Photocatalysis: Fundamentals and Applications*, ed. N. Serpone and E. Pelizzetti, Wiley, New York, 1989.
21 N. Serpone, D. Lawless, R. Terzian and D. Meisel, in *Electrochemistry in Colloids and Dispersions*, ed. R. A. Mackay and J. Texter, VCH, New York, 1992, ch. 30, pp. 399–416.
22 C. S. Turchi and D. F. Ollis, *J. Catal.*, 1990, **122**, 178.
23 C. Boxall and G. H. Kelsall, *J. Chem. Soc., Faraday Trans.*, 1991, **87**, 3547.
24 G. Rothenberger, J. Moser, M. Grätzel, N. Serpone and D. K. Sharma, *J. Am. Chem. Soc.*, 1985, **107**, 8054.
25 D. Duonghong, E. Borgarello and M. Grätezel, *J. Am. Chem. Soc.*, 1981, **103**, 4685.
26 J. Moser and M. Grätzel, *Helv. Chim. Acta*, 1982, **65**, 1436.
27 D. Duonghong, J. Ramsden and M. Grätzel, *J. Am. Chem. Soc.*, 1982, **104**, 2977.
28 M. A. Fox, B. Lindig and C. C. Chen, *J. Am. Chem. Soc.*, 1982, **104**, 5828.
29 J. Moser, M. Grätzel, D. K. Sharma and N. Serpone, *Helv. Chim. Acta*, 1985, **68**, 1686.
30 J. Moser, M. Grätzel and R. Gallay, *Helv. Chim. Acta*, 1987, **70**, 1596.
31 R. B. Draper and M. A. Fox, *Langmuir*, 1990, **6**, 1396.
32 J. M. Warman, M. P. Haas, P. Pichat, T. P. M. Koster, E. A. van der Zouwen-Assink, A. Mackor and R. Cooper, *Radiat. Phys. Chem.*, 1991, **37**, 433.
33 J. M. Warman, M. P. de Haas, P. Pichat and N. Serpone, *J. Phys. Chem.*, 1991, **95**, 8858.
34 J. M. Warman, M. P. de Haas, M. Grätzel and P. P. Infelta, *Nature (London)*, 1984, **310**, 306.
35 K. M. Schindler and M. Kunst, *J. Phys. Chem.*, 1990, **94**, 8222.
36 R. W. Fessenden and P. V. Kamat, *Chem. Phys. Lett.*, 1986, **123**, 233.
37 J. M. Warman and M. P. de Haas, in *Pulse Radiolysis*, ed. Y. Tabata, CRC Press, Boca Raton, 1991, ch. 6.
38 M. Kunst and G. J. Beck, *Appl. Phys.*, 1986, **60**, 3558.
39 P. P. Infelta, M. P. de Haas and J. M. Warman, *Radiat. Phys. Chem.*, 1977, **10**, 353.
40 G. Lepore, C. H. Langford, J. Víchová and A. Vlcek, *J. Photochem. Photobiol. A: Chem.*, 1993, **75**, 67.
41 R. I. Bickley, T. Gonzalez-Carreno, J. S. Lee, L. Palmisano and R. J. D. Tilley, *J. Solid State Chem.*, 1991, **92**, 178.
42 *Degussa Technical Bulletin No. 56*, 1990.
43 A. L. Pruden and D. F. Ollis, *J. Catal.*, 1983, **82**, 404.
44 C. Y. Hsiao, C. L. Lee and D. F. Ollis, *J. Catal.*, 1983, **82**, 418.
45 M. Barbeni, E. Pramauro, E. Pelizzetti, E. Brogarello, M. Grätzel and N. Serpone, *Nouv. J. Chem.*, 1984, **8**, 547.
46 D. F. Ollis, C. Y. Hsiao L. Budiman and C. L. Lee, *J. Catal.*, 1984, **88**, 89.
47 M. Barbeni, E. Pramauro and E. Pelizzetti, *Chemosphore*, 1985, **14**, 195.
48 M. Barbeni, E. Pramauro and E. Pelizzetti, *Chemosphere*, 1986, **15**, 1913.
49 R. W. Matthews, *Aust. J. Chem.*, 1987, **40**, 667.
50 R. W. Matthews, *J. Catal.*, 1988, **111**, 264.
51 H. Al-Ekabi, N. Serpone, E. Pelizzetti and C. Minero, *Langmuir*, 1989, **5**, 250.
52 R. Terzian, N. Serpone, C. Minero, E. Pelizzetti and H. Hidaka, *J. Photochem. Photobiol. A: Chem.*, 1990, **55**, 243.
53 C. Kormann, D. W. Bahnemann and M. R. Hoffmann, *Environ. Sci. Technol.*, 1991, **25**, 494.
54 H. Hidaka, K. Nohara, J. Zhao, N. Serpone and E. Pelizzetti, *J. Photochem. Photobiol. A: Chem.*, 1992, **64**, 247.
55 E. Pramauro, M. Vincenti, V. Augugliaro and L. Palmisano, *Environ. Sci. Technol.*, 1993, **27**, 1790.
56 G. Mills and M. R. Hoffmann, *Environ. Sci. Technol.*, 1993, **27**, 1681.
57 J. C. D'Oliveira, G. Al-Sayyed and P. Pichat, *Environ. Sci. Technol.*, 1990, **24**, 990.
58 J. Cunningham and S. Srijaranai, *J. Photochem. Photobiol. A: Chem.*, 1988, **43**, 329.
59 G. Al-Sayyed, J. C. D'Oliveira and P. Pichat, *J. Photochem. Photobiol. A: Chem.*, 1991, **58**, 99.
60 K. Okamoto, Y. Yamamato, H. Tanaka, M. Tanaka and A. Itaya, *Bull. Chem. Soc. Jpn.*, 1985, **58**, 2015.
61 M. Barbeni, M. Morello, E. Pramauro and E. Pelizzetti, *Chemosphere*, 1987, **16**, 1165.
62 A. Mills, S. Morris and R. Davies, *J. Photochem. Photobiol. A: Chem.*, 1993, **70**, 183.
63 A. P. Y. Durand, D. Brattan and R. G. Brown, *Chemosphere*, 1992, **25**, 783.
64 C. Boxall and G. H. Kelsall, *J. Chem. Soc., Faraday Trans.*, 1991, **87**, 3537.
65 K. Johansson, R. Cowdery, M. O'Neil, J. Rehm and G. McLendon, A. Marchetti and D. G. Whitten, *Isr. J. Chem.*, 1993, **33**, 67.
66 R. Rossetti, J. L. Ellison, J. M. Gibson and L. E. Brus, *J. Chem. Phys.*, 1984, **80**, 4464.
67 R. Rossetti, R. Hull, J. M. Gibson and L. E. Brus, *J. Chem. Phys.*, 1985, **83**, 1406.
68 Y. Nosaka, N. Ohta and H. Miyama, *J. Phys. Chem.*, 1990, **94**, 3752.
69 W. L. Wilson, P. F. Szajowski and L. E. Brus, *Science*, 1993, **262**, 1242.
70 H. Gerischer, in *Physical Chemistry: An Advanced Treatise*, ed. H. Eyring, Academic Press, London, 1970, vol. IXA, Electrochemistry, ch. 5, p. 463.
71 P. Wardman, *J. Phys. Chem. Ref. Data*, 1989, **18**, 1637.
72 S. G. Bratsch, *J. Phys. Chem. Ref. Data*, 1989, **18**, 1.
73 G. Redmond, A. O'Keefe, C. Burgess, C. MacHale and D. Fitzmaurice, *J. Phys. Chem.*, 1993, **97**, 11081.
74 K. Mizushima, M. Tanaka and S. Iida, *J. Phys. Soc. Jpn.*, 1972, **32**, 1519.
75 K. Mizushima, M. Tanaka, K. Asai and K. Iida, *AIP Conf. Proc.*, 1973, **18**, 1044.
76 K. Mizushima, M. Tanaka, A. Asai, S. Iida and J. B. Goodenough, *J. Phys. Chem. Solids*, 1979, **40**, 1129.
77 S. R. Morrison, *Electrochemistry at Semiconductor and Oxidized Metal Electrodes*, Plenum Press, New York, 1980.
78 H. O. Finklea, in *Semiconductor Electrodes*, ed. H. O. Finklea, Elsevier, New York, 1988, p. 52.
79 A. Liu, M. C. Sauer and A. D. Trifunac, *J. Phys. Chem.*, 1993, **97**, 11265.
80 R. A. Marcus and N. Sutin, *Biochim. Biophys. Acta*, 1985, **811**, 265.
81 R. A. Marcus, *J. Phys. Chem.*, 1990, **94**, 1050.
82 M. Anpo, T. Shima, S. Kodama and Y. Kubokawa, *J. Phys. Chem.*, 1987, **91**, 4305.
83 H. Gerischer and A. Heller, *J. Phys. Chem.*, 1991, **95**, 5261.
84 H. Gerischer and A. Heller, *J. Electrochem. Soc.*, 1992, **139**, 113.

Paper 4/02297A; *Received* 18*th April*, 1994